ELSEVIER

#### Contents lists available at ScienceDirect

# Solar Energy

journal homepage: www.elsevier.com/locate/solener





# Analysis of the impact of high-flux irradiation in accelerated aging testing of solar absorber coatings

Sahar Hosseini <sup>a</sup>, Mahdiar Taheri <sup>a</sup>, Shuang Wang <sup>a</sup>, Inmaculada Cañadas <sup>b</sup>, Aránzazu Fernández-García <sup>b</sup>, Kaoru Tsuda <sup>c</sup>, Florian Sutter <sup>d</sup>, Simon Caron <sup>d</sup>, Antonio Tricoli <sup>e</sup>, Wojciech Lipiński <sup>f</sup>, Juan F. Torres <sup>a</sup>, Joe Coventry <sup>a,\*</sup>

- <sup>a</sup> School of Engineering, Australian National University, Canberra, ACT 2601, Australia
- <sup>b</sup> CIEMAT-Plataforma Solar de Almería, Ctra. Senés, Km 4, P.O. Box 22, 04200 Tabernas, Almería, Spain
- <sup>c</sup> Nano Frontier Technology, 3-10-6-105, Osaki, Shinagawa-ku, Tokyo, Japan
- d DLR German Aerospace Center, Institute of Solar Research, Calle Doctor Carracido Nr. 44, 1st floor, 04005 Almería, Spain
- <sup>e</sup> Nanotechnology Research Laboratory, Faculty of Engineering, University of Sydney, Sydney 2050, Australia
- f The Cyprus Institute, 2121 Nicosia, Cyprus

#### ARTICLE INFO

# Keywords: Accelerated aging Absorber coating High-flux irradiation Concentrating solar thermal Optical degradation

#### ABSTRACT

Solar absorber coatings play a critical role in concentrating solar thermal (CST) plants by impacting receiver efficiency. To study the lifetime of coatings, they are typically subjected to accelerated aging tests using various methods. In this study, thermal cycling tests designed to simulate the effects of cloud passage were conducted using three methods: (1) a furnace method using a vertical split tube furnace; (2) an on-sun flux method using a solar furnace; (3) and a simulated flux method using a high-flux solar simulator. The simplest of these three methods, cycling heating in a programmable furnace, avoids the requirement for a concentrated radiation source. The main aim of the testing was to compare these methods and understand if high-flux irradiation impacts the optical degradation rate. After 500 cycles (around 62 h of total testing time) using the simulated flux method and 300 cycles (around 40 h of total testing time) using the on-sun flux method, the maximum difference in solar absorptance between these two high-flux methods and the furnace test method was less than 0.3 %, a result consistent for both coating types tested in this study, Pyromark and a coral-structured coating. We suggest the effects of UV radiation or operating with higher flux gradients across samples may not be important to aging characteristics of coatings, and that the simpler furnace test method may be sufficient for many applications.

# 1. Introduction

A solar absorber coating is a crucial component of a receiver in a concentrating solar thermal (CST) plant. Such coatings degrade over several years of operation, leading to increased reflection and emission losses from receivers [1–3], thereby decreasing receiver efficiency over time [4]. To determine their lifetime and potential reasons for their optical and mechanical degradation, solar absorber coatings are typically subjected to accelerated aging tests [5–7]. Various accelerated aging tests, including isothermal (IT) and thermal cycling (TC) tests, have been reported in the literature. IT and TC tests assess the impact of exposure time, temperature [3,5,6], and cyclical thermal stress from cloud passage [8–10] on coating degradation.

Torres et al. [8] studied the changes in Pyromark, a well-known

commercial high-temperature absorber coating, under IT and TC aging tests. Rapid-cycling ("RC") and cycle-and-hold ("CH") tests were selected as the cycling patterns for the TC tests. In the CH test, the sample temperature was varied between 550 °C and 850 °C, and held at the upper temperature for 285 s in each cycle. The RC test had similar temperature parameters, but no holding time at the maximum temperature. The results revealed that the absorptance variation in CH tests had a distinct trend compared to the other tests. Hosseini et al. [10] studied the impact of different conditions in RC and CH tests, such as holding time, ramp rate, and temperature, on the degradation and failure of the coatings. The results showed that frequent thermal stress changes coupled with holding time at the maximum temperature (CH tests) accelerated the absorptance drop and change in morphology and crystallography. Their findings also revealed that the CH test cannot be replaced by consecutive (but separate) IT and RC tests, with the same

E-mail address: joe.coventry@anu.edu.au (J. Coventry).

https://doi.org/10.1016/j.solener.2025.113978

Received 8 May 2025; Received in revised form 20 August 2025; Accepted 7 September 2025 Available online 15 September 2025

<sup>\*</sup> Corresponding author.

| Nomenclature               |  | $T_{\mathrm{ave}}$        | Temporal average of temperature (°C)  |  |  |
|----------------------------|--|---------------------------|---|--|--|
|                            |  | TC                        | Thermal cycling test  |  |  |
| Latin letters              |  | $T_{\max}$                | Maximum temperature during the cycle (°C)   |  |  |
| CH                         | Cycle and hold aging test  | $T_{\min}$                | Minimum temperature during the cycle (°C)   |  |  |
| $G_{\mathrm{s},\ \lambda}$ | Solar spectral irradiance from ASTM G173-03 (W m <sup>-2</sup>       | x                         | Normalised pixel density in the fitted curve  |  |  |
| ,                          | $nm^{-1}$ )  | y                         | Flux value in the fitted curve (W $m^{-2}$ )  |  |  |
| IT<br>HFSS                 | Isothermal aging test<br>High Flux Solar Simulator                   | Greek letters             |   |  |  |
| L <sub>a</sub>             | Lamp number "a" in HFSS  | $\alpha$                  | Solar absorptance   |  |  |
| RC                         | Rapid cycling test   | $\alpha_{\lambda,\theta}$ | Spectral directional absorptance  |  |  |
| S                          | Location of samples in the sample holder used for the on-            | σ                         | Stefan–Boltzmann constant (5.67 $\times$ 10 <sup>-8</sup> W m <sup>-2</sup> K <sup>-4</sup> ) |  |  |
| J                          | sun flux test  | λ                         | Wavelength (nm)   |  |  |
| s <sup>'</sup>             | ***************************************                              | $ ho_{\lambda}$           | Spectral reflectance  |  |  |
| <b>ડ</b>                   | Location of samples in the sample holder used for the HFSS flux test | $\theta$                  | Incidence angle in XRD  |  |  |
| T                          | Temperature (K)  |                           |   |  |  |

total holding time and cycle numbers. Therefore, they suggested subjecting new absorber coatings to CH tests for comprehensive durability analysis.

Many other studies have also included aging tests in various types of programmable furnaces [9,11–13]. However, only a few studies have attempted to incorporate the impact of concentrated solar irradiation. Boubault et al. [14] investigated absorptance variation of Pyromark after 3000 s of on-sun TC tests using a high-flux solar accelerated aging facility. This setup utilised heliostats and a parabolic concentrator to concentrate sunlight onto the samples. Air flowing behind the samples controlled temperature and caused a temperature gradient through the samples. During the test, the samples experienced different flux levels, from  $104 \text{ kW m}^{-2}$  to  $340 \text{ kW m}^{-2}$ , with cycle periods of 10 or 30 s. Their findings indicated that exposure irradiance levels and holding time both had an influence on coating absorptance degradation, i.e. Pyromark absorptance dropped more in tests with higher exposure irradiance and holding time However, due to the relatively short testing duration (the total testing time was less than 3000 s or  $1\,$  h), no significant degradation and failure was observed. Reoyo-Prats et al. [15] also conducted on-sun TC tests using the same setup as Boubault et al. [14] where samples were held at both the maximum and minimum temperatures, with testing up to 200 cycles. The testing time for each cycle duration was around 5 min, and total testing time was around 17 h. In their test, the temperature of the samples was varied between 400 °C and 800 °C, with corresponding flux variation from 250 kW m<sup>-2</sup> to 700 kW m<sup>-2</sup>. They suggested that future testing should have longer duration as they did not observe any significant degradation.

Caron et al. [16] subjected different tubular-shaped coated samples to an on-sun test using a solar dish for up to 100 cycles. During these cycles, sample temperature was varied between 200 °C and 650 °C, with a 30-minute holding time at the upper temperature, and gradual ramp rate of 30 K min<sup>-1</sup>. In these tests, the coatings were exposed to flux ranging from 40 kW m<sup>-2</sup> to 250 kW m<sup>-2</sup> and the temperature of the samples was controlled by adjusting the airflow inside the tube. No significant optical degradation was observed in the coatings subjected to these tests, which had total duration of around 100 h. Martínez-Manuel et al. [17] investigated the photo-thermal efficiency of various coatings, using Pyromark as a benchmark, under two different solar flux levels,  $100 \pm 3$  kW m<sup>-2</sup> and  $415 \pm 12$  kW m<sup>-2</sup>, during a short exposure period (1.5 h) using a high-flux solar simulator. In this setup, xenon lamps simulated solar radiation, and the irradiance on the samples was controlled by a curtain placed between the lamps and the samples. A calorimetric test bench was employed to maintain stable sample temperatures throughout the experiment. The results showed that the efficiency of coatings decreased with increasing flux, and Pyromark exhibited the highest absorptance degradation-about 1.22 % over the test duration.

A drawback of all these high-flux tests to-date is that the aging period is relatively short, ranging from 50 min to 17 h for high-temperature tests (800 °C), or up to 100 h for tests at a slightly lower temperature (650 °C). This is mainly due to the cost and complexity involved in the testing, where the facility is usually required to be attended by an operator. Clear conclusions about whether or not high flux is important to the mechanisms of coating degradation are yet to be drawn, possibly as a result of the brief testing duration, which in terms of accumulated time represents a small fraction of that typical for furnace tests, which might run for thousands of hours. In the present work, similar limitations are faced in terms of testing complexity and therefore the duration of testing, although the duration of our testing conducted at 800°C was four times longer than those conducted by Reoyo-Prats et al. [15]. However, to address this limitation, in addition to optical characterisation (absorptance measurement) we focus on understanding the underlying aging mechanisms through in-depth materials analysis, comparing the results from high-flux testing with other, longer-duration tests carried out in programmable furnaces. Early signs of degradation can be expected to be seen by this approach, even for relatively short duration tests.

Concentrated irradiation causes a steep thermal gradient across a coating, that develops rapidly assuming the back side of the sample is subject to cooling. Although thermal gradients across samples may be obtained in furnace-based testing (e.g. [8,10]), the effect of the non-isothermal condition during the whole aging process has not been studied in furnace tests. The impact of the latter effect on the aging mechanism and, consequently, optical and mechanical durability as compared to furnace-based testing, is examined in the present study. Furthermore, the potential effect of irradiation by the highly energetic UV photons in the concentrated solar spectrum on the aging mechanism of high-temperature solar absorber coatings is scrutinised. In our previous work [10], we identified the CH test as a critical test with which to evaluate coating performance, as it accelerates degradation relative to the IT and RC tests.

The objective of this work is to determine whether the addition of high-flux radiation (from solar flux or solar-simulated flux) significantly affects the optical and mechanical durability of coatings during durability testing. Many researchers have worked to develop absorber coatings with improved stability and efficiency compared to Pyromark [3,18,19]. It is important to determine which types of accelerated aging tests should be conducted to allow for meaningful comparisons of their durability during operation. In our previous work [10], we showed that IT is a suitable first step, but it is not sufficient on its own. Subsequent testing under thermal cycling conditions is necessary to evaluate coating stability under temperature fluctuations. As thermal cycling can be conducted using different methods, including conventional laboratory furnaces [7,8], on-sun tests using solar furnaces or dishes [20,21], and

high-flux solar simulators (HFSS) [17], our primary aim here is to develop a better understanding of whether solar irradiance has a significant impact on coatings degradation.

Conventional laboratory furnaces would provide a simpler and more cost-effective alternative to concentrated radiation facilities. The significance of this work lies in its potential to reduce the complexity and cost of testing solar absorber coatings while still delivering reliable and meaningful results. To achieve this, we replicate conventional CH (cyclic heating) testing procedures but introduce concentrated radiation exposure. Experiments were conducted at the CIEMAT-Plataforma Solar de Almería (PSA) using the solar furnace (SF40) and at the Australian National University (ANU) using the high-flux solar simulator (HFSS), and results were compared to CH tests previously performed at ANU in a programmable furnace. Our aim is to develop further understanding of whether accelerated aging tests can be reliably performed in a conventional laboratory furnace, which offers a cheaper and simpler alternative to concentrated radiation facilities. The significance of this work lies in its potential to simplify and reduce the cost of testing solar absorber coatings while maintaining accurate results. In the present work, only one flux level has been studied and the effect of varying heat flux level on coatings degradation is out of scope.

#### 2. Materials and methods

#### 2.1. Samples

Two different solar absorber coatings were investigated in this study: (1) Pyromark and (2) a coral-structured coating. The coatings were deposited on 30 mm  $\times$  30 mm  $\times$  3 mm metallic substrates. Pyromark was painted on Inconel 625 (Inc625) by the method described in [2]. The coral-structured coating was deposited on Inc625 and stainless steel 316L (SS316L) with details of the method provided in [17,18]. This multi-layer coating comprises a base layer for enhancing adhesion between layers, a coral-shaped absorption layer for improving absorptance using the light trapping in its macro- and micro-porous structures, and a top-layer consisting of silica nano-spheres to improve absorptance by light scattering [13]. The coral-structured coating shows higher photothermal efficiency and durability compared to Pyromark from both extensive IT [18] and TC [10] tests. The aim of using two different coatings was to determine the impact of various testing methods on coatings with quite different structures.

#### 2.2. Characterisation

Solar absorptance is the primary optical property of interest for absorber coatings [1]. Its impact on receiver efficiency is more significant than thermal emittance [22]. For example, a 1 % decrease in absorptance leads to a 1 % reduction in the photo-thermal energy conversion efficiency of the coating, while a 10 % increase in emittance results in a 1 % decrease in efficiency [15,22]. This influence becomes even less pronounced in systems with high concentration ratios, such as central tower CSP systems, where the ratio typically exceeds 1000 suns [22,23]. As the effect of emittance is less than absorptance in central tower CSP systems, in this study the focus is on solar absorptance degradation, and changes in thermal emittance is beyond the scope. Therefore, the focus here was on solar absorptance degradation, with changes in thermal emittance beyond the scope of this study. After some number of aging cycles, samples were cooled to room temperature and removed from the testing setup for optical characterisation. A Perkin Elmer UV/VIS/NIR Lambda 1050 spectrophotometer with a 150 mm InGaAs integrating sphere (constant angle of incidence, 8°) was used to measure the spectral reflectance of samples ranging from 280 to 2500 nm. Since samples do not allow light to pass through them, the spectral absorptance  $(\alpha_{\lambda})$  can be calculated by  $\alpha_{\lambda} = 1 - \rho_{\lambda}$ , where  $\rho_{\lambda}$  is the measured spectral reflectance. Solar absorptance is calculated as:

$$\alpha = \frac{\int_{280 \text{nm}}^{2500 \text{nm}} \alpha_{\lambda,\theta} G_{\text{s},\lambda} d\lambda}{\int_{280 \text{nm}}^{2500 \text{nm}} G_{\text{s},\lambda} d\lambda},$$
(1)

where  $\alpha_{\lambda,\theta}$ ,  $\lambda$ , and  $G_{s,\lambda}$  are the spectral directional absorptance, the wavelength (nm), and the solar spectral irradiance (W m $^{-2}$  nm $^{-1}$ ) from the ASTM G173-03 direct reference spectrum at Air Mass 1.5, respectively.

Material characterisation was carried out on the coated samples. Changes in morphology were studied using a scanning electron microscope (SEM, Zeiss UltraPlus) at different magnifications. The changes in crystalline structure and the formation of new phases in coatings during the aging were studied by an X-ray diffraction system (XRD, D2 Phaser Bruker) using a Cu-K $\alpha$  radiation source ( $\lambda_{average}=1.54059$  Å). The  $2\theta$  range was set from 8 to  $80^{\circ}$ .

#### 2.3. Accelerated aging test methods

Each of the three testing campaigns is based on the cycle and hold (CH) test, attempting to achieve similar temperature ranges, ramp rates and hold times. Under real operating conditions, numerous factors influence coating efficiency; however, it is challenging to account for all of them simultaneously in a single test. Therefore, in these tests, certain aspects—such as temperature gradients during operation—were intentionally simplified to allow a clearer focus on the main objective, investigating the impact of flux, and other dominant factors like temperature and thermal stress. These methods include a furnace method using a vertical split furnace; an on-sun high-flux method using a solar furnace at CIEMAT-PSA; and a simulated-sun high-flux method at ANU. Further details of these methods are explained as follows.

#### 2.3.1. Furnace method

The first method utilises a vertical split tube furnace with a stainless steel sample holder for CH tests as described in [8]. TC testing was carried out in previous work for up to 5000 cycles [10]. Compared to IT and RC testing, the CH test was shown to significantly influence the rate of coating degradation and absorptance drop, as well as the nature of morphological and phase changes (see Fig. 3 and Fig. 4 in [10]). One of the CH tests (the CH-285 s test in [10]) was chosen as the benchmark test, and test conditions in the high-flux campaigns were matched to this insofar as possible. In the CH furnace test, the sample temperature was varied between 600°C and 800°C with a heating and cooling rate of 3 K s<sup>-1</sup> and a holding time of 285 s at 800 °C for each cycle. Heating was achieved both convectively from air within the furnace, and radiatively from the surrounding furnace walls, and cooling was carried out using a cold air jet impinging on the rear of the samples (while the furnace was still on and hot). As a result of the air jet, during the cooling stage there is a reasonably significant temperature gradient through the sample (refer to Fig. S3 in [10]) not seen in the heating stage. To the best of our knowledge, there is no published data on the actual cooling rates of CSP absorber coatings under real-world conditions. Data on direct normal irradiance fluctuations and simulation results suggest a cooling rate of approximately 1.5 °C s<sup>-1</sup> at the maximum temperature point on the receiver tube [24], although anecdotal evidence indicates that ramping rates can occasionally be faster, exceeding 25 K s<sup>-1</sup>. While testing at very high cooling rates could provide further insights, a rate of 3 K s<sup>-1</sup> was selected to ensure consistent control across all methods and to enable comparison between different aging procedures, rather than to explore the influence of extreme cooling conditions. Notably, this cooling rate falls within the range used in previous studies [8,9,16]. The testing method described here using the vertical split furnace is referred to as the furnace method in this paper.

### 2.3.2. On-sun flux method

Samples underwent on-sun testing using a high-concentration solar furnace (SF40) at CIEMAT-PSA. Fig. 1 shows a schematic diagram and

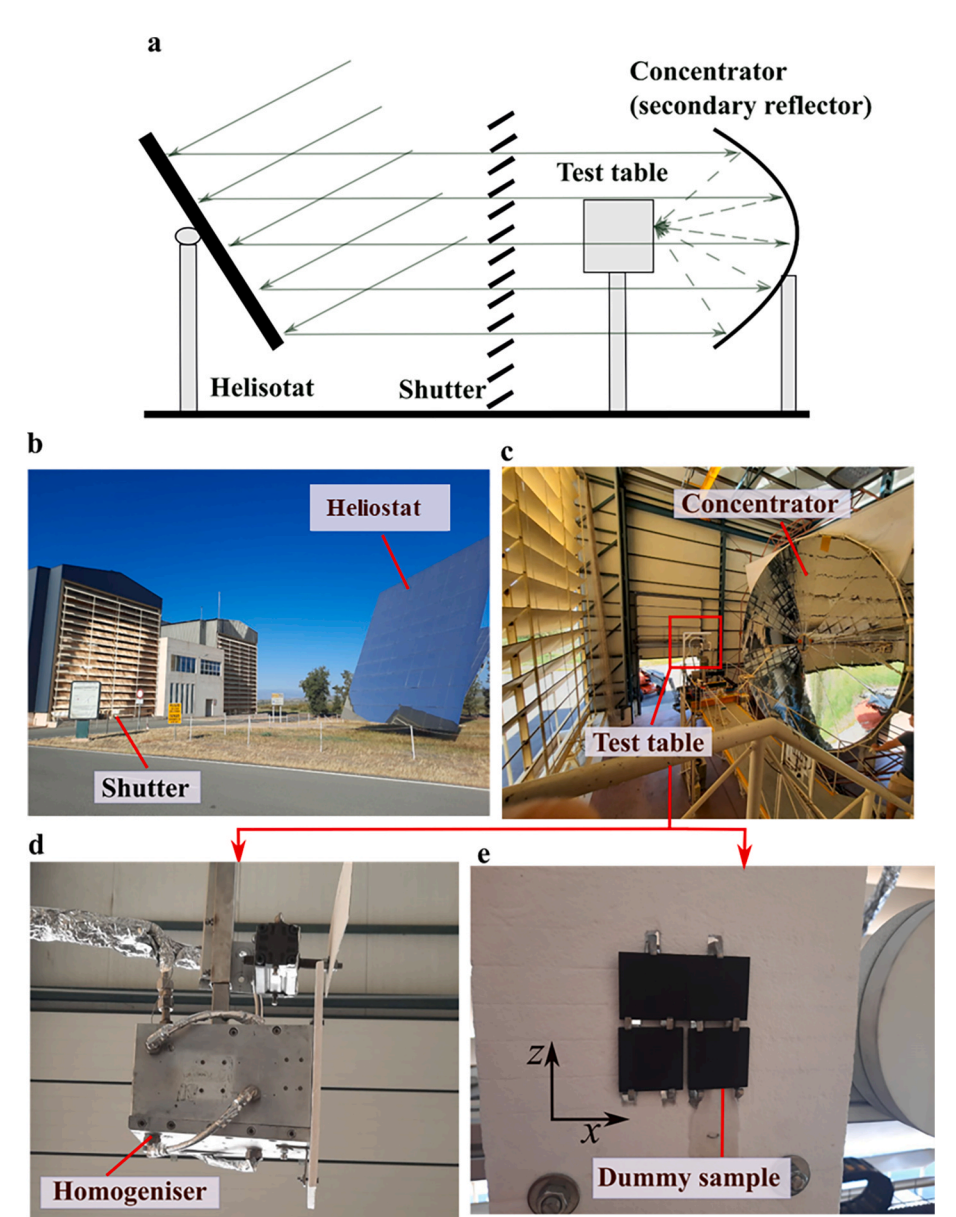


**Fig. 1.** On-sun flux method using the solar furnace (SF-40) located at CIEMAT-PSA: (a) schematic of SF-40, and (b–e) photos of different parts of the furnace: (b) heliostat and shutter, (c) concentrator and test table, (d) a solar flux homogeniser, and (e) sample holder with three testing samples and a dummy sample. The coordinate system referred to in this study (*z* and *x* directions) is shown adjacent to the samples.

photos of the SF-40 facility. This furnace comprises a 100 m $^2$  flat heliostat, which tracks the sun and reflects light to a fixed parabolic dish concentrator inside a building, with an 8.5 m diameter [25]. A shutter between the heliostat and the parabolic concentrator is used to control the intensity of the solar radiation in the focal region, from a maximum concentration of 7000  $\times$  down to a selected level. This method is referred to as the *on-sun flux* method in this study.

To have a uniform flux distribution on samples, a trapezoidal homogeniser was placed in the focal region. The homogeniser walls are covered with highly reflective silvered-glass mirrors and are cooled by a water-cooling system (Fig. 1d). A ceramic sample holder was positioned at the back of the homogeniser, designed to accommodate four samples (Fig. 1e). The edges of the samples were held by metal pins without contacting the sample holder. One of the samples, Pyromark on Inc625, was selected as a dummy sample and included thermocouples mounted in three holes drilled laterally into the substrate, each with a diameter of about 1 mm and positioned about 15 mm in from the edge (Fig. 2b). The dummy sample temperature ( $T_3$  measured by TC<sub>3</sub>) was used for control

(as described further below). Furthermore, as the three test samples do not have their own temperature sensor, they were assumed to have the same temperature as the dummy sample. This assumption potentially introduces error in the experiments, and therefore the uncertainty in temperature between samples is discussed further below.

Two coral-structured coatings on SS316L and Inc625, along with Pyromark on Inc625, underwent CH-285 s tests for up to 300 cycles. Fig. 2 shows the temperature profile and temperature gradient through the dummy sample during the CH-285 s tests. Since there was no active cooling system behind the samples, the holding temperature and cooling stage were only controlled by adjusting the shutter and relying on natural convection cooling at the back of the samples. To reach and maintain the temperature of the samples at 800°C, the shutter was opened by 15–20 %. Keeping it open by 5–8 % resulted in the temperature of samples reaching 600 °C, with a cooling rate of 2 K s $^{-1}$  (the average cooling rate for 20 cycles). The cooling rate in the furnace test was slightly higher at 3 K s $^{-1}$ . However, a previous work [10] indicates that doubling the cooling rate (3 K s $^{-1}$  vs 6 K s $^{-1}$ ) has a minor effect on

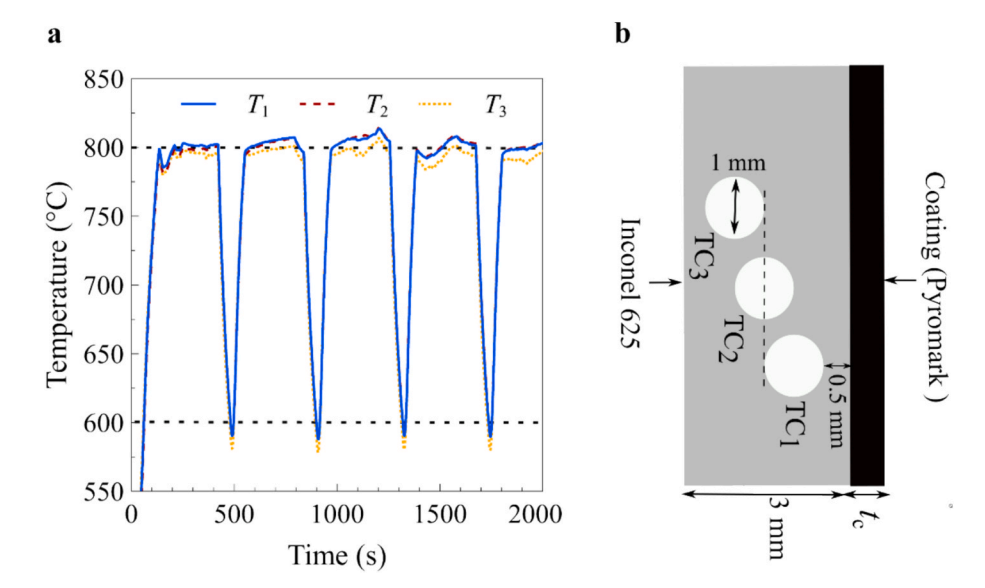


**Fig. 2.** Temperature measurements using the dummy sample during the CH-285 s on-sun test: (a) transient temperature profiles at three thermocouple locations and (b) schematic representation of the side-view of the dummy sample, indicating the thermocouple locations.

the coatings' degradation after 5000 cycles. Therefore, the impact of this difference (2 K s $^{-1}$  versus 3 K s $^{-1}$ ) is not expected to significantly impact the test results. The temperature gradient across the samples (i.e.  $T_1-T_3$ , from thermocouples  $\rm TC_1$  and  $\rm TC_3$  respectively, Fig. 2b) differed between the methods during the tests. This discrepancy can be attributed to variations in the testing methods. Further results and explanation regarding the temperature difference through samples under these various methods are reported in Table S1.

The flux received by the samples was measured using a flux gauge (Vatell Corporation), which scanned different areas at the back of the homogeniser. This measurement was conducted at intervals of 10 mm in both the x and z directions (shown in the insert of Fig. 1e and Fig. S1). Fig. 3 shows the flux distribution measured and reveals that it was not entirely uniform. This non-uniform flux is believed to be due to a combination of uneven optical properties/characteristics of the reflectors in the solar furnace (age/degradation related, mirror alignment, etc), combined with dimensional characteristics of the homogeniser. The maximum flux on the samples reached 240 kW m<sup>-2</sup> with variation down to 120 kW m<sup>-2</sup> in certain areas. The temperature at TC<sub>3</sub> (Fig. 2b) was used for control purposes, and the total average of flux at the homogeniser exit when TC3 reached 800 °C and 600 °C was 193.0  $\pm$  32.0 and 95.0  $\pm$  15.0 kW m<sup>-2</sup>, respectively. The individual samples did not experience precisely the same flux values (Fig. 3) and the average flux received by each sample is reported in Table 1. Sample S2, a coral-

**Table 1** Average flux measured for different samples at 800  $^{\circ}$ C and their average surface temperature during the holding process measured using an infrared camera and a thermocouple behind the samples. Note these individual sample temperature measurements were only taken during setup. During testing, the temperature signal is taken from the instrumented dummy sample, and used for all samples despite the known discrepancies.

| Name  | S <sub>1</sub> (Coralstructured coatings on Inc625) | S <sub>2</sub> (Coralstructured coatings on SS316L) | S <sub>3</sub><br>(Pyromark<br>on Inc625) | S <sub>4</sub><br>(Dummy<br>sample) |
|---|---|---|---|-------------------------------------|
| Flux (kW m <sup>-2</sup> )  | $181.8\pm20.5$                                      | $213.9\pm12.6$                                      | $211\pm14.7$                              | 198.4 ± 29.4                        |
| Temperature<br>measured by an<br>infrared camera<br>of the coating<br>surface (°C)    | 830   | 850   | 840                                       | 835                                 |
| Temperature<br>measured by a K-<br>type<br>thermocouple<br>behind the<br>samples (°C) | 700   | 770   | 750                                       | 730                                 |

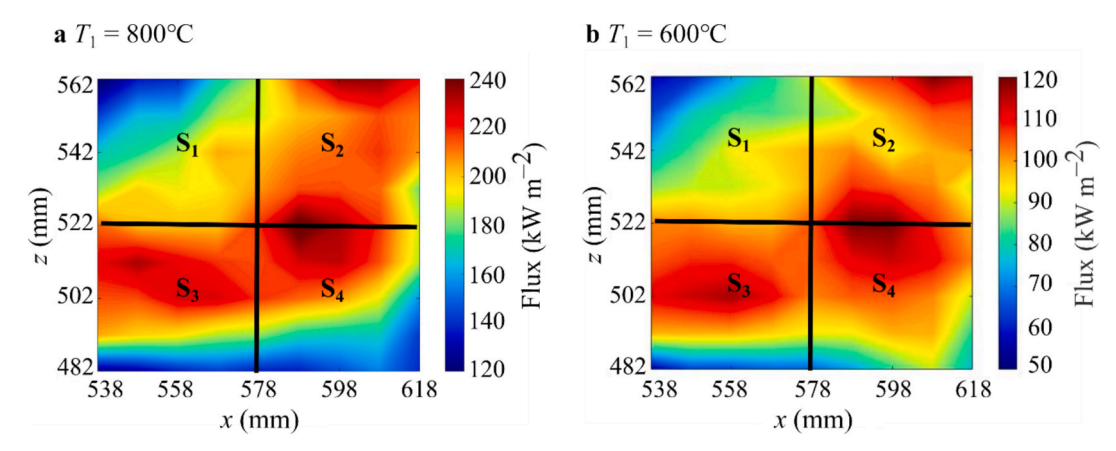


Fig. 3. Flux map of concentrated sunlight on samples when the dummy sample temperature measured by TC<sub>1</sub> in Fig. 2b reached (a) 800 °C and (b) 600 °C.

structured coating on SS316L, was exposed to the highest flux, while sample  $\mathrm{S}_1$ , corresponding to a coral-structured coating on Inc625, was under the lowest flux. The discrepancy in their average flux value was about 32 kW m $^{-2}$ .

Since the average flux on the samples was not uniform, a variation in the temperatures of the samples was anticipated. To quantify this variation a comparison was made between the temperature of samples (including the dummy sample) using thermocouples mounted on the rear side during the test and also using an infrared camera with an assumption of 100 % of emittance (default camera setting) for the coatings. Table 1 reports the samples' temperature during the holding stage. It is acknowledged that there is significant uncertainty in the resulting temperature values, due to errors inherent in both methods including contact resistance between thermocouples and the back side of samples, the calibration of the camera, the difference in the emittance value for samples, and changes in emittance during aging. Nonetheless, these methods can still be valuable for quantitative comparison of temperature between different samples, and significant variation is observed. For example, the coral-structured coating on Inc625 (or S<sub>1</sub> in Fig. 3) experienced the minimum temperature with as much as a 70°C difference relative to the other samples (Table 1). This result also indicates that the temperature of the coatings is higher than it was for the tests in the furnace method (i.e. higher than 800°C). For example, the comparison of  $T_1$  measured by a thermocouple inside the dummy samples (S<sub>4</sub>) with the temperature measured by the infrared camera from the coating surface showed that the surface temperature was around 35 °C hotter. However, temperature differences of less than 50 °C are unlikely to cause significant variations in these coatings degradation [7,18]. For instance, degradation of coatings at temperatures of 800 °C and 850 °C after 1000 h of aging would result is less than 0.5 % change for coralstructured coatings and Pyromark [7,18]. Therefore, it is assumed that the temperature variation of coatings surface in different samples can be neglected and assumed to be consistent across all samples as these temperature variations between samples are not lower than 50 °C (Table 1).

#### 2.4. HFSS flux method

In the simulated flux method, the ANU high-flux solar simulator (HFSS) was used to simulate the CH-285 s test with approximately the same conditions as the other methods. The HFSS comprises 18 radiation modules (Fig. 4a), each equipped with a 2.5 kWe xenon short-arc lamp, a truncated elliptical-shaped reflector (Fig. 4b), and an air-cooling system behind the lamp. These modules were aligned to focus light at the same point [26,27]. The lamps are turned on at 24.7 V and different currents, i.e. 50 A, 70 A, 85 A, and 100 A out of the maximum 100 A. They require at least 10 min after being turned on to reach steady conditions. A calibrated metal-oxide-semiconductor camera is employed for monitoring and capturing images of the focal plane and samples. It is also used to measure the radiative flux distribution on a water-cooled Lambertian target (Haueter Engineering GmbH) coated with alumina with dimensions of 35 cm imes 35 cm [28]. To measure the flux value, a Lambertian target with a heat flux gauge (Vatell Corporation, TG1000-0 series) at its centre (Fig. 4b) is used. The water circulation also serves to cool the flux gauge. The diameter of the flux gauge sensor is 1.52 mm. Further details of the system can be found in [29]. In this paper, this method is called the HFSS flux method.

Based on the relationship between the pixel intensity in the photo of the flux distribution on the Lambertian target and the flux measured in the sensor area, the flux map for other areas can be obtained using the method explained in [29]. This method involved initially measuring the flux values in the focal plane at the centre (i.e. the focal point) and at 20 points laterally in the focal plane, up to approximately  $\pm 22.5$  mm away from the centre (in the direction shown by red dots in the insert of Fig. 4c). Then, the plain Lambertian target is replaced by the flux gauge, and the images capturing the flux distribution are obtained. The

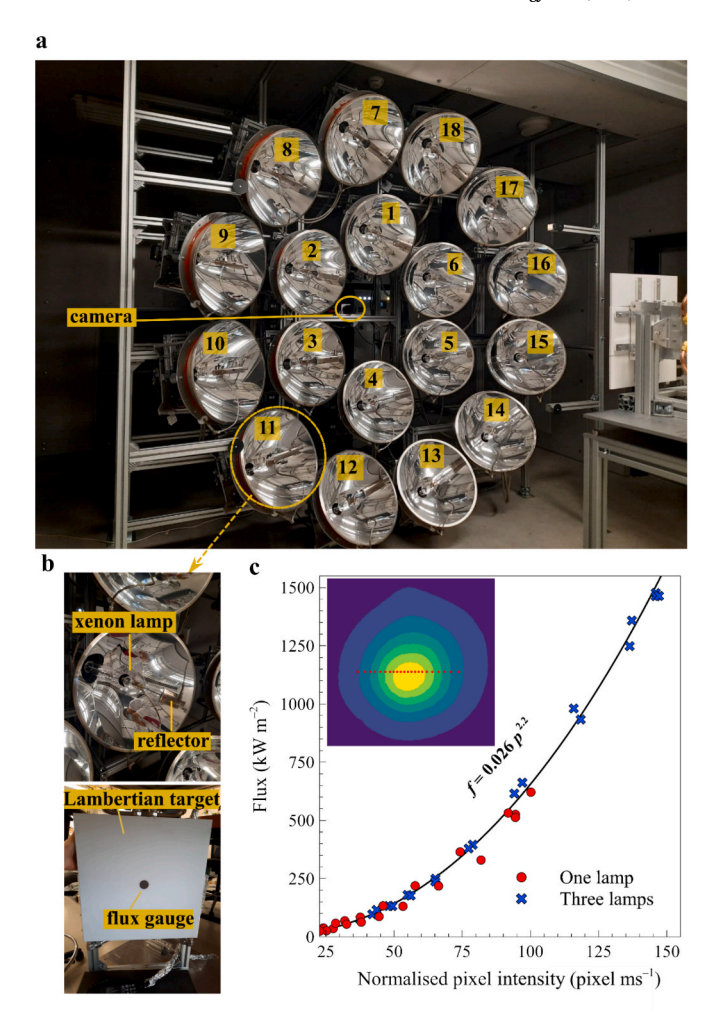


**Fig. 4.** HFSS test: (a) HFSS setup, (b) xenon lamp and Lambertian target with flux gauge, and (c) relation between normalised pixel intensity and measured flux value with 25 ms of exposure time with one  $(L_3)$  and three lamps  $(L_1, L_3,$  and  $L_6)$  with 100 A current setting on the lamps. Each data point was measured at different positions in the focal plane, from the centre (focal point) up to  $\pm 22.5$  mm from the centre. In the fitted curve, f is the flux value and p is the normalised pixel intensity.

movement of the Lambertian target and flux gauge was facilitated using a linear actuator.

Fig. 4 shows the relation between flux values and normalised pixel intensities with the exposure time (i.e. pixel intensity/exposure time) setting for the camera for one lamp and three lamps. The exposure time of camera was set for 25 ms for this experiment. The result shows a consistent trend between flux value and normalized pixel intensity for both scenarios, and this trend can be accurately represented by a power curve ( $y = 0.026 \, x^{2.2}$ , where y is the flux value and x is the normalised pixel intensity). Utilising this curve fitting, the flux map for the entire area can be generated. A similar analysis was conducted for another exposure time (15 ms) for one, three, and six lamps, as depicted in Fig. S2. When all six lamps are operating at maximum current (100 A), the focal point is exposed to around 3500 kW m<sup>-2</sup> [29] (equivalent to 3500 suns, Fig. S3).

Due to the small size of the focal spot (compared to our samples), and the significant flux gradient close to the focal point, a homogeniser is essential to give more uniform flux on the samples when testing absorber coatings. Therefore, a trapezoidal–shaped homogeniser was built (Fig. 5a), based on a design from the National Renewable Energy Laboratories [30] and positioned with its entrance at the focal plane. The homogeniser walls are made of stainless steel and incorporate a water-

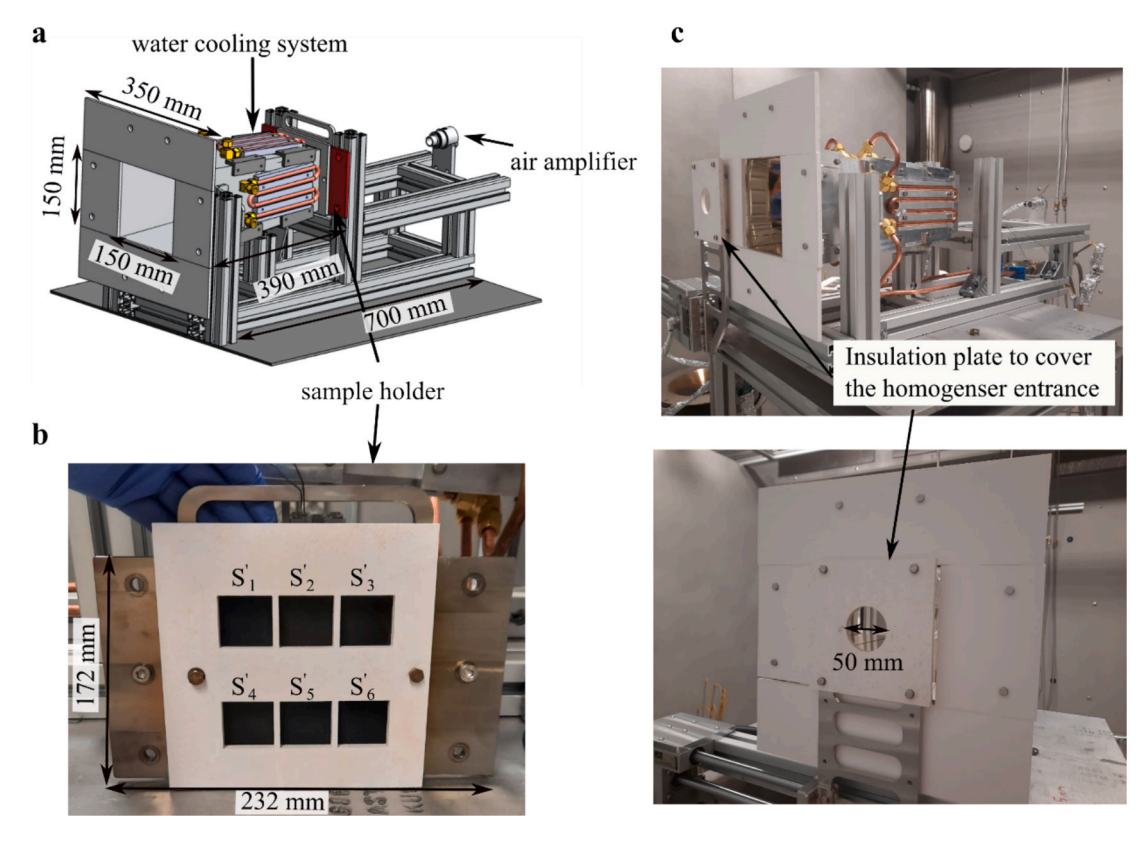
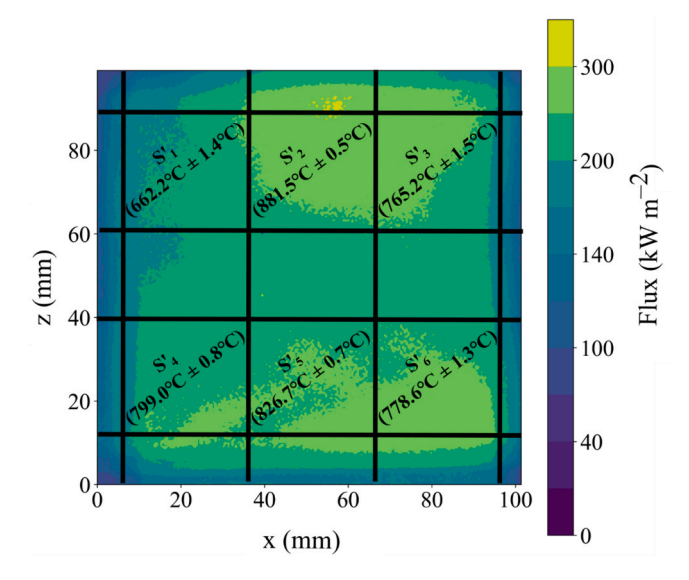


Fig. 5. Homogeniser for the HFSS test: (a) schematic of the overall homogeniser/sample holder assembly, (b) sample holder with six samples (with each sample labelled), (c) a photo of the whole setup and the ceramic shield used in the cooling stage for covering the homogeniser entrance.

cooling system on each side to maintain a low temperature for both the walls and the attached mirrors. 1 mm thick low-iron solar mirror glass was attached to the inside walls of the homogeniser using a relatively high temperature resistant adhesive (3 M Hi-Strength 90 Spray Adhesive). At the rear side of the homogeniser, a stainless-steel sample holder was positioned (with a small gap between it and the homogeniser to avoid heat conduction), accommodating up to six coating samples (Fig. 5b). An air amplifier (NEX-40000 Adjustable Air Amplifier) with a proportional pressure controller (0.6–7 bar) was used to blow air onto the back side of the sample holder to regulate the samples' temperature during the cooling and holding processes (Fig. 5a). Fig. 5c shows a photo of the homogeniser after assembly.

To achieve a cooling rate close to 2–3 K s<sup>-1</sup>, consistent with previous testing methods, a ceramic shield (ZIRCAR refractory sheet type RSLE-57) covered a part the homogeniser entrance to reduce the amount of flux received by the samples (Fig. 5c). The flux shielding is combined with cooling from the air jet at the back of the samples to reduce their temperature by 200 °C. Given the extremely high flux on the focal plane (e.g. up to 3500 suns for six lamps with 100 A), a hole was left in the ceramic shield in the centre region to prevent it from damage (Fig. 5c).

Fig. 6 shows the distribution of flux using six lamps ( $L_1$ – $L_6$  in Fig. 4a, set at 70 A) at the locations of the samples, with their flux values derived from the correlation explained earlier. Relatively good uniformity is observed, significantly better than for the solar furnace tests, but still with a level of variation. The flux distribution for each lamp (Fig. S4) covers a section of each of the samples' area, and results in a relatively uniform flux distribution when combined as six lamps together (Fig. 6). Increasing the lamp current leads to higher flux values on the samples, although not in a linear way (Fig. S5). For instance, for 70 A (Fig. 6 and Fig. S5b), the maximum flux reached around 350 kW m $^{-2}$  in a local region, with an average of  $224 \pm 40$  kW m $^{-2}$ . This value increased to a peak of 600 kW m $^{-2}$  and an average of  $392 \pm 70$  kW m $^{-2}$  for 100 A (Fig. S5). The aim was to achieve relatively similar flux conditions to the



**Fig. 6.** Flux distribution at sample locations when using six lamps  $(L_1-L_6)$  set to 70 A (the average stable temperature for each location is given in the superimposed text).

on-sun flux method, and for this purpose, six lamps with a current of 70 A were selected. On average, the flux values on samples were in the range  $200-250 \text{ kW m}^{-2}$  (Fig. S5).

Based on our observations from the on-sun flux method (Fig. 3 and Table 1), an increase of about 32 kW  $\rm m^{-2}$  in flux increased samples' temperature by about 70 °C. In contrast, here there was a significant difference between the temperature of samples, up to 200 °C (Fig. 6 and Fig. S6), while the average flux difference between them was not

substantially different from the on-sun tests (Fig. 6). The reason is believed to be due to heat losses from conduction between the sample holder and its support frame, necessitating a re-design in future experiments. Due to this conduction, there is a temperature gradient laterally, with cooler regions closer to the sides, which is where the support frame attaches. The temperature in each sample test position was measured by rotating the instrumented dummy sample into each of the six positions, under constant test conditions. In subsequent work, it is recommended that the steel sample holder be replaced with a material of lower thermal conductivity, preferably non–metal, or configured as for the on-sun flux method with minimum contact to samples (e.g. with holder pins).

Therefore, despite the relatively uniform flux distribution between samples, the temperature of the samples was not as well controlled as in the furnace method. Hence, in this test, only S<sub>4</sub>, S<sub>5</sub>, and S<sub>6</sub> sample positions were selected as they were closest to each other in temperature (Fig. 6). As can be seen in Fig. 7, the samples' temperatures can be considered on average as around 800 °C  $\pm$  50 °C. The samples chosen for S<sub>4</sub>, S<sub>5</sub>, and S<sub>6</sub> were Pyromark on Inc625, coral-structured coating on Inc625, and coral-structured coating on SS316L, respectively. During the heating phase, there was no air flow onto the back side of samples. During the holding time, the air flow at the rear of the samples was set to 45 L per minute, and during cooling, at 115 L per minute, resulting in an average cooling rate of  $2 \pm 0.2$  K s<sup>-1</sup>, closely aligned with the conditions in previous tests. Although it is understood that in real-world applications, fluids such as molten salts or thermal oils with higher heat capacities are typically used, here air cooling is employed to enable effective temperature control and monitoring without the added complexity of fluid-loop systems. This approach has also been adopted in previous studies [8,14,21].

Based on our previous work, most of the absorptance degradation occurred within the first 1000 cycles for both coatings under furnace testing conditions [10]. Therefore, 1000 cycles were targeted as the benchmark for this study. However, the on-sun and HFSS tests were more complex to set up and operate, making it challenging to reach this cycle number within the current timeframe. Therefore, the focus was placed on the initial degradation.

#### 3. Results and discussion

#### 3.1. Solar absorptance

Fig. 8 illustrates the variation in the solar absorptance of samples

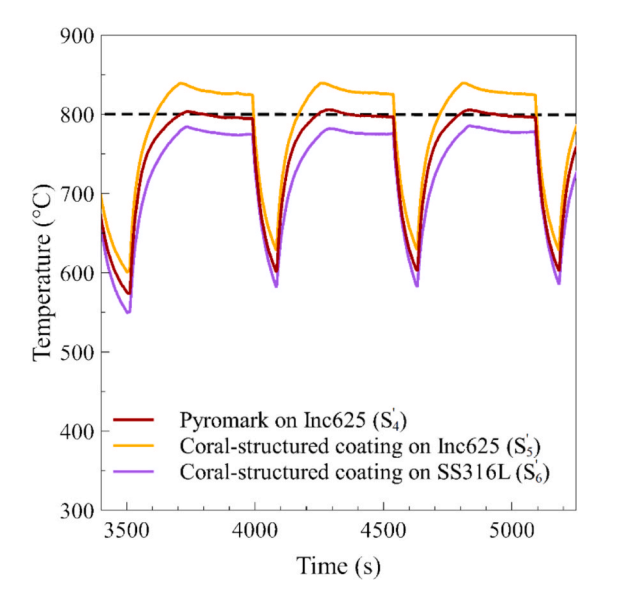


Fig. 7. Temperature profile of  $S_4$ ,  $S_5$ , and  $S_6$  during the tests with six lamps set to 70 A.

undergoing the CH-285s tests (under almost the same conditions) via different methods. Initial absorptance values of samples were not precisely the same due to variations in the deposition process, and therefore they were normalised with their initial values for comparison purposes (Table. S2). Referring first to the results for the coral-structured coating on Inc625 (Fig. 8a), we see similar trends between the tests conducted in the furnace and the on-sun flux method. Both experienced an initial fall in solar absorptance by 0.4 % and then stayed stable. However, for the HFSS test, absorptance had an initial larger drop (around 0.6 % after 100 cycles) and then slightly increased before stabilising at 0.5 %. The larger absorptance drop can be explained by the sample experiencing a higher coating temperature in testing when compared to the other methods (Fig. 7 and Table 1). For the second coating sample, the coral-structured coating on SS316L (Fig. 8b), a different trend is observed. Here the initial absorptance drops for the on-sun and HFSS flux tests were similar (0.5 % difference in the first 100 cycles), followed by a stable phase, whereas for the furnace testing the initial drop was somewhat lower. The reason for this trend is unknown, but many factors could contribute to it, such as temperature and flux distribution, as well as temperature gradients within these samples. In the final case, Pyromark on Inc625 (Fig. 8c), there is a consistent downward trend in absorptance for all three test methods. However, the sample tested under HFSS flux exhibited relatively stable absorptance after 200 cycles. The underlying reasons for this behaviour are not yet clear and require further investigation. As coral-structured coatings are not cured before aging, the different initial absorptance drop observed between methods may be attributed to their temperature difference or the heating method, rather than an indication of long-term trends.

The maximum difference in absorptance degradation between these three methods was within 0.3 % based on data from 500 cycles of the simulated flux method and 300 cycles of the on-sun flux method (Fig. 8). This difference was consistent across the different samples. Although a more extended test duration is recommended for a conclusive assessment, these initial results suggest that the impact of inclusion of high flux (whether on-sun or from a simulator) compared to a simpler furnace test may be negligible, from which we infer that effects of UV radiation or operating with higher flux gradients across samples may not be important to aging characteristics of coatings. This observation is consistent with observations from the material characterisation testing explained later.

Fig. 9 compares the absolute value of solar absorptance between Pyromark and coral-structured coatings deposited on the same substrate (Inc625) during the CH-285s aging conducted by these different testing methods. Regardless of the testing method, the absolute value of absorptance for the coral-structured coating remained significantly higher than Pyromark during aging (1.8 % higher for furnace tests after 800 cycles, and about 1.4 % higher for tests using on-sun flux and simulated flux methods). The coral-structured coating remained stable after the initial drop observed in the first 100 cycles, whereas Pyromark exhibited a continuous downward trend throughout the entire 800 cycles.

#### 3.2. Material characterisation

Fig. 10 shows top-view SEM images of the coral-structured coating and Pyromark on Inc625 before and after the CH-285 s aging test under different numbers of cycles. During aging, the changes in morphology and phase formation can be observed. After 2500 cycles of CH-285 s furnace testing, Pyromark exhibited changes in morphology such as sintering and crystallisation, while the coral-structured coating remained morphologically stable (Fig. 10b and Fig. S7). After 300 cycles of tests using simulated flux and on-sun flux methods, no significant changes were observed for both coatings (Figs. 10c and d). However, the size and number of cracks changed during aging. An SEM image of the samples after 300 cycles under the furnace method was not taken but, based on other CH test results with holding time of 120 s, would not be

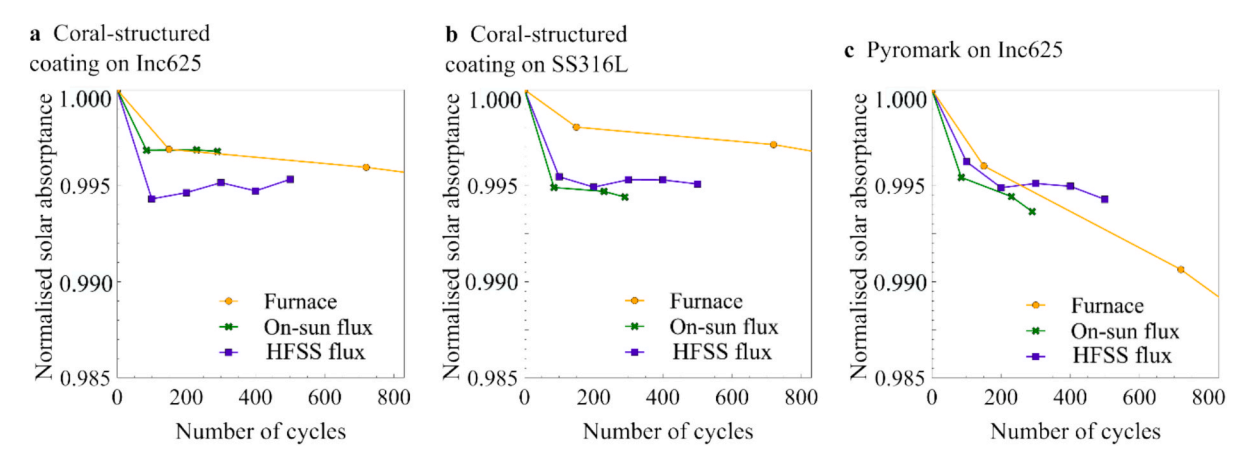
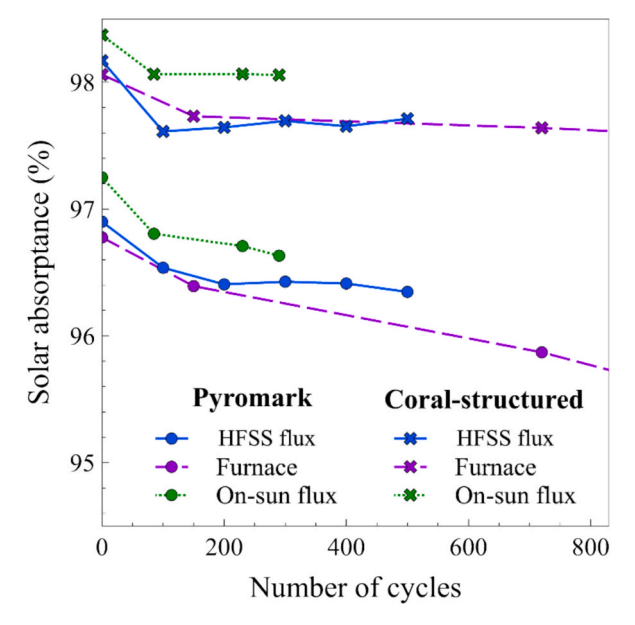


Fig. 8. Comparison of solar absorptance variation for samples of (a) coral-structured coatings on Inc625, (b) coral-structured coatings on SS316L, and (c) Pyromark on Inc625, during the CH-285 s aging test using the furnace, on-sun flux, and simulated flux methods.



**Fig. 9.** Comparison of solar absorptance of coral-structured coatings and Pyromark on Inc625 during the CH–285 s aging test using different test methods.

expected to show any significant change. In these tests no significant morphological change was observed after 2500 cycles, corresponding to a total holding time of 84 h, which is 40 h longer than the current tests with 300 cycles ([10]). Therefore, the initial signs of change are expected to appear after more than 300 cycles, which was the maximum tested in this study. To draw definitive conclusions, additional testing using flux-based methods over extended cycles is recommended to verify whether the morphological changes observed in Pyromark under the furnace method are reproducible with other testing methods.

At low magnification, signs of failure were observed in some parts of the coral-structured coating on SS316L after 300 cycles of testing by onsun flux and 300 cycles of testing by simulated flux (red arrows in Fig. 11). In contrast, this failure was not observed after 2500 cycles of furnace testing. This discrepancy can be attributed to non-uniform flux distribution within samples, resulting in higher local temperatures in some areas. Both the high- and low-magnification SEM images of coral-structured coatings on Inc625 after 500 cycles of simulated flux did not show any significant changes or signs of failure (Fig. S8).

Fig. 12 shows the XRD pattern of Pyromark and coral-structured coatings undergoing these testing methods. The coral-structured

coatings on Inc625 exhibit the same peaks for the tests with different methods (Fig. 12a), indicating that the high-flux methods did not affect the material phases in this coating for up to 500 cycles of testing. The same observation is made for this coating on SS316L (Fig. S9). Pyromark on Inc625, after 2500 cycles of testing in the furnace (Fig. 12b), displays peaks related to the formation of new phases (both P<sub>1</sub> and P<sub>2</sub>) discussed in [2]. However, only P<sub>1</sub> was observed for the HFSS flux and on-sun flux methods. This is the first phase formed after initial aging but converts into another phase (P2) after either a longer aging time or exposure to higher temperature during the isothermal aging test [2]. A thick layer of Pyromark paint was heated in an alumina crucible, and it was shown that both phases formed even in the absence of any substrate. Therefore, the appearance of this phase results solely from the aging of the coating itself. Further details can be found in [2]. This phase also appeared during the cycle-and-hold tests after a shorter holding time compared to isothermal aging tests conducted at the same temperature [10]. Therefore, it is expected that this phase transformation would be observed for the other methods were they to be tested for a longer duration.

#### 4. Conclusions

In this study, the degradation rates of high-temperature absorber coatings were investigated comparatively using a thermal 'cycle-andhold' test in a furnace, an on-sun test using a solar furnace, and a labbased high-flux solar simulator test. The tests conducted in the furnace reveal the impact of exposure time, temperature, and thermal stress on coating degradation but overlook the potential impact of concentrated solar flux, where samples are exposed to UV radiation and experienced steep temperature gradients from high flux on one side. The on-sun flux and simulated flux tests aimed to simulate conditions closer to what might be experienced in a real plant. Controlling the conditions was challenging, i.e. achieving consistent uniform flux and temperature across different test samples. Nonetheless, the two different kinds of high-flux tests were able to replicate the conditions of the selected cycleand-hold CH-285 s test reasonably well. Results were obtained for 500 cycles (equivalent to 62 h of total testing time), which is around four times the duration of previous work at a similarly high temperature range, with test samples cycling in a temperature range between 600°C and 800°C with a 285 s holding time at the upper temperature. Measurements of solar absorptance indicated comparable degradation trends between the three different testing methods, with a difference of only 0.3 % observed for the 500 cycles (around 62 h of total testing time) of testing under the simulated flux method and the 300 cycles (around 40 h of total testing time) of testing under the on-sun flux method, across two coating types. Similarly, results from materials characterisation, both in terms of morphological and phase changes, indicated little

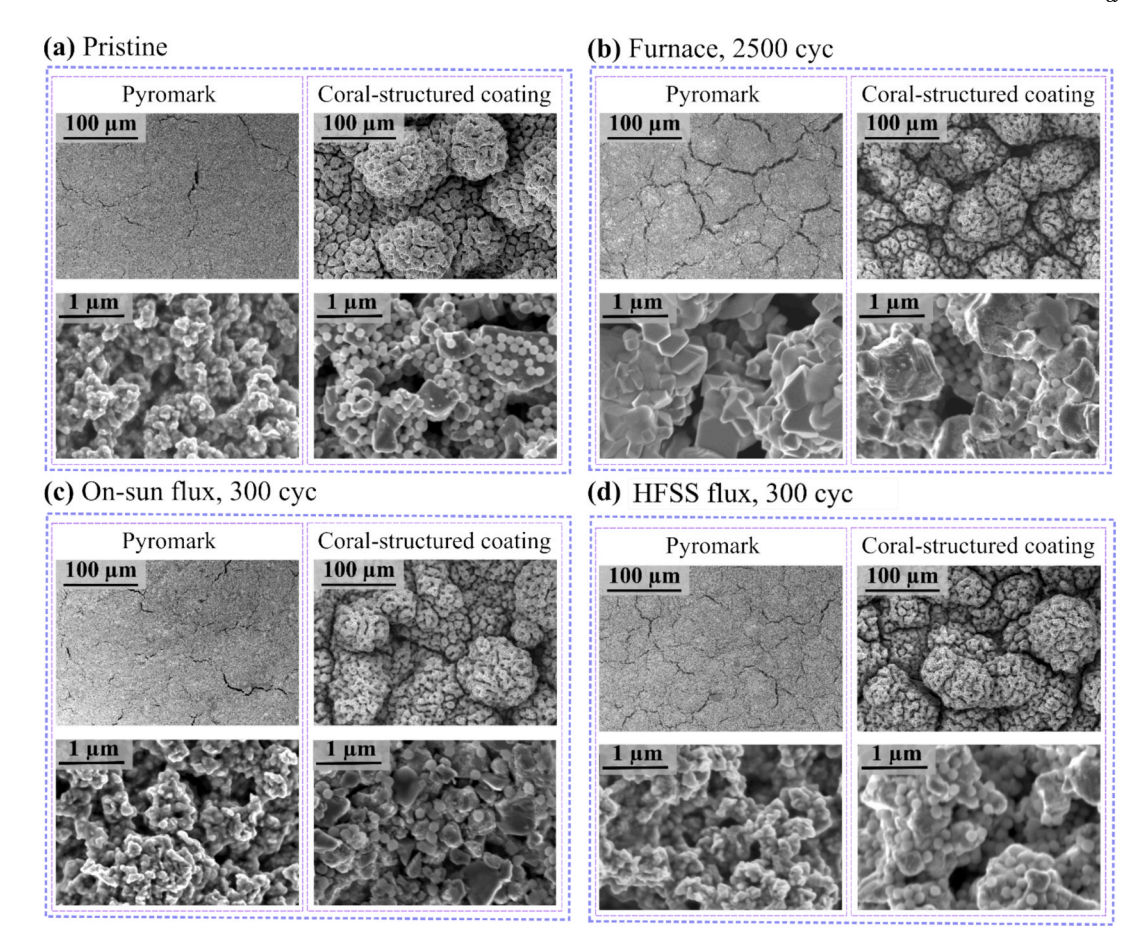


Fig. 10. SEM images of Pyromark and coral-structured coatings on Inc625: (a) before aging, and (b–d) after aging using different methods: (b) furnace after 2500 cycles, (c) on-sun flux after 300 cycles, and (d) HFSS flux after 300 cycles.

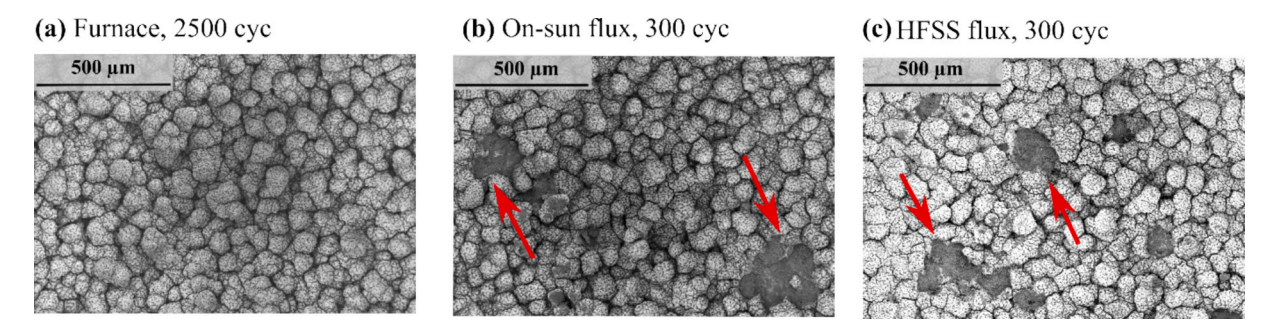


Fig. 11. Low magnification of SEM images of coral-structured coatings on SS316L after aging using different methods: (a) furnace after 2500 cycles, (b) on-sun flux after 300 cycles, and (c) HFSS flux after 500 cycles.

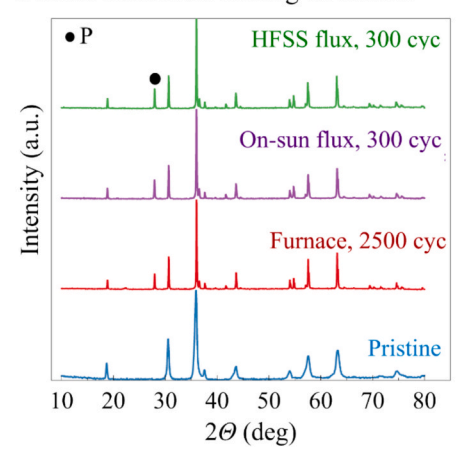
difference between the three testing methods. The findings suggest that, despite minor discrepancies, testing from the simpler cycle-and-hold furnace test method can adequately represent the results one might expect from the more complex and costly on-sun flux and simulated flux testing, in the first hours of aging. This suggests that for the initial evaluation of newly developed coatings over a limited number of cycles, as demonstrated in [17,20,31], furnace-based TC tests can serve as a suitable replacement for more complex testing methods. This work was an early-stage investigation, and to have final conclusions regarding long-term degradation mechanisms, extended testing over longer durations is necessary. Several main recommendations for further work are (a) improving the design of the homogeniser and experimental setup to achieve a more uniform flux distribution across samples and thereby increase the reliability of the tests; (b) continued, longer duration testing

using the high-flux methods, for further comparison with furnace tests, (c) on-sun and/or solar simulator high-flux testing at flux levels exceeding the 200–250 kW m $^{-2}$  levels competed so far, perhaps up to around 500–600 kW m $^{-2}$  typical of fluxes on the hottest regions near the exit of current solar towers [32], (d) using a fluid-loop system for cooling and maintaining constant sample temperatures during testing to enable the investigation of the impact of temperature gradients that are more representative of real operating conditions on coating degradation, (e) investigating the variation in thermal emittance of absorber coatings during aging under high solar flux conditions.

# CRediT authorship contribution statement

Sahar Hosseini: Writing – original draft, Methodology,

#### a Coral-structured coating on Inc625



#### **b** Pyromark on Inc625

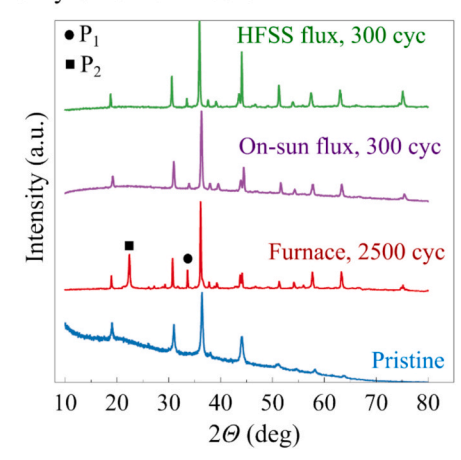


Fig. 12. Comparison of XRD pattern of coatings undergoing the different testing methods: (a) coral-structured coating on Inc625, and (b) Pyromark on Inc625.

Investigation, Formal analysis, Conceptualization. Mahdiar Taheri: Writing – review & editing, Methodology, Investigation. Shuang Wang: Methodology, Investigation. Inmaculada Cañadas: Methodology, Investigation. Aránzazu Fernández-García: Writing – review & editing, Methodology, Investigation, Conceptualization. Kaoru Tsuda: Resources, Investigation. Florian Sutter: Writing – review & editing, Methodology, Investigation. Simon Caron: Writing – review & editing, Methodology, Investigation. Antonio Tricoli: Supervision, Funding acquisition. Wojciech Lipiński: Writing – review & editing, Supervision, Funding acquisition. Juan F. Torres: Writing – review & editing, Supervision, Project administration, Investigation, Funding acquisition, Conceptualization. Joe Coventry: Writing – review & editing, Supervision, Project administration, Investigation, Funding acquisition, Conceptualization.

#### Declaration of competing interest

The authors declare that they have no known competing financial interests or personal relationships that could have appeared to influence the work reported in this paper.

#### Acknowledgements

This research was founded by the Australian Research Council (ARC) Linkage Project LP170101239. Funding from industry partners Vast Solar and Nano Frontier Technology is gratefully acknowledged. The authors acknowledge the facilities, and the scientific and technical assistance of the Australian Microscopy Facility at the Centre of Advanced Microscopy (CAM) at the Australian National University. The authors also wish to thank Judy Netter and the team in the High Flux Solar Furnace Laboratory at the National Renewable Energy Laboratory for sharing the design of their flux homogeniser. Finally, we extend our thanks to the team of the Centro de Investigaciones Energéticas, Medioambientales y Tecnológicas (CIEMAT) and the German Aerospace Center (DLR) at the CIEMAT-Plataforma Solar de Almería for their contributions and assistance in conducting the on-sun testing.

## Appendix A. Supplementary data

Supplementary data to this article can be found online at https://doi.org/10.1016/j.solener.2025.113978.

#### References

[1] C. K. Ho, A. R. Mahoney, A. Ambrosini, M. Bencomo, A. Hall, and T. N. Lambert, "Characterization of Pyromark 2500 paint for high-temperature solar receivers," in

- Proceedings of the ASME 2012 6th International Conference on Energy Sustainability, San Diego, USA, 2012, p. 91374.
- [2] S. Hosseini, J.F. Torres, M. Taheri, A. Tricoli, W. Lipiński, J. Coventry, Long-term thermal stability and failure mechanisms of Pyromark 2500 for high-temperature solar thermal receivers, Sol. Energy Mater. Sol. Cells 246 (2022) 111898, https:// doi.org/10.1016/j.solmat.2022.111898.
- [3] E.B. Rubin, Y. Chen, Solar energy materials and solar cells optical properties and thermal stability of Cu spinel oxide nanoparticle solar absorber coatings, Sol. Energy Mater. Sol. Cells 195 (February) (2019) 81–88.
- [4] M. López-Herraiz, A.B. Fernández, N. Martinez, M. Gallas, Effect of the optical properties of the coating of a concentrated solar power central receiver on its thermal efficiency, Sol. Energy Mater. Sol. Cells 159 (2017) 66–72.
- [5] T.K. Kim, et al., Copper-alloyed spinel black oxides and tandem-structured solar absorbing layers for high-temperature concentrating solar power systems, Sol. Energy 132 (2016) 257–266.
- [6] R.K.J. Moon, T.K. Kim, B. Vansaders, C. Choi, Z. Liu, S. Jin, et al., Black oxide nanoparticles as durable solar absorbing material for high-temperature concentrating solar power system, Sol. Energy Mater. Sol. Cells 134 (2015) 417–424, https://doi.org/10.1016/j.solmat.2014.12.004.
- [7] S. Hosseini, et al., Long-term thermal stability testing of the CoteRill®750 solar absorber coating, AIP Conf. Proc. (2021).
- [8] J.F. Torres, I. Ellis, J. Coventry, Degradation mechanisms and non-linear thermal cycling effects in a high-temperature light-absorber coating, Sol. Energy Mater. Sol. Cells 218 (2020) 110719.
- [9] L. Noč, et al., High-solar-absorptance CSP coating characterization and reliability testing with isothermal and cyclic loads for service-life prediction, Energy Environ. Sci. 12 (5) (2019) 1679–1694.
- [10] S. Hosseini, et al., Aging mechanisms for high-temperature solar absorber coatings under extensive thermal cycling, Sol. Energy Mater. Sol. Cells 271 (Jul. 2024) 112856, https://doi.org/10.1016/j.solmat.2024.112856.
- [11] C.K. Ho, A.R. Mahoney, A. Ambrosini, A. Hall, T.N. Lambert, Characterization of Pyromark 2500 paint for high-temperature solar receivers, Sol. Energy Eng. 136 (February) (2014) 1–6.
- [12] S. Hosseini, J.F. Torres, M. Taheri, A. Tricoli, W. Lipiński, J. Coventry, Stability and characterisation of Pyromark 2500 cured at different temperatures, Sol. Energy 265 (Nov. 2023) 112102, https://doi.org/10.1016/j.solener.2023.112102.
- [13] Y. Guo, et al., Scalable nano-architecture for stable near-blackbody solar absorption at high temperatures, Nat. Commun. 15 (1) (Jan. 2024) 384, https://doi.org/10.1038/s41467-023-44672-3.
- [14] G. Boubault, A. Claudet, B. Faugeroux, O. Olalde, Aging of solar absorber materials under highly concentrated solar fluxes, Sol. Energy Mater. Sol. Cells 123 (2014) 211–219, https://doi.org/10.1016/j.solmat.2014.01.010.
- [15] R. Reoyo-Prats, et al., Accelerated aging of absorber coatings for CSP receivers under real high solar flux – Evolution of their optical properties, Sol. Energy Mater. Sol. Cells 193 (January) (2019) 92–100.
- [16] S. Caron et al., "Accelerated ageing of solar receiver coatings: Experimental results for T91 and VM12 steel substrates," presented at the SolarPACES 2017: International Conference on Concentrating Solar Power and Chemical Energy Systems, Santiago, Chile, 2018, p. 230002. doi: 10.1063/1.5067230.
- [17] L. Martínez-Manuel, et al., A comprehensive analysis of the optical and thermal performance of solar absorber coatings under concentrated flux conditions, Sol. Energy 239 (Jun. 2022) 319–336, https://doi.org/10.1016/j.solener.2022.05.015.
- [18] J.F. Torres, et al., Highly efficient and durable solar thermal energy harvesting via scalable hierarchical coatings inspired by stony corals, Energy Environ. Sci. (2022).
- [19] R. Harzallah, M. Larnicol, C. Leclercq, A. Herbein, and F. Campana, "Development of high performances solar absorber coatings," AIP Conf. Proc., vol. 2126, no. July, 2019, doi: 10.1063/1.5117538.
- [20] A. Boubault, C. K. Ho, A. Hall, T. N. Lambert, and A. Ambrosini, "Durability of solar absorber coatings and their cost-effectiveness," Sol. Energy Mater. Sol. Cells, vol. 166, no. November 2016, pp. 176–184, 2017.

- [21] S. Caron et al., "Forty shades of black: A benchmark of high temperature sprayable black coatings applied on Haynes 230," AIP Conf. Proc., vol. 2303, no. December, 2020, doi: 10.1063/5.0028773.
- [22] S. Caron, J. Garrido, J. Ballestrín, F. Sutter, M. Röger, F. Manzano-Agugliaro, A comparative analysis of opto-thermal figures of merit for high temperature solar thermal absorber coatings, Renew. Sustain. Energy Rev. 154 (Feb. 2022) 111818, https://doi.org/10.1016/j.rser.2021.111818.
- [23] S. Caron, et al., Laboratory intercomparison of solar absorptance and thermal emittance measurements at room temperature, Sol. Energy Mater. Sol. Cells 238 (2022), https://doi.org/10.1016/j.solmat.2022.111579.
- [24] F. Crespi, A. Toscani, P. Zani, D. Sánchez, G. Manzolini, Effect of passing clouds on the dynamic performance of a CSP tower receiver with molten salt heat storage, Appl. Energy 229 (Nov. 2018) 224–235, https://doi.org/10.1016/j. apenergy.2018.07.094.
- [25] F. Buendía-Martínez, F. Sutter, S. Gledhill, D. Argüelles-Arízcun, I. Cañadas, A. Fernández-García, Innovative lifetime testing protocol for high-temperature secondary reflector materials used in concentrated solar thermal energies, Sol. Energy Mater. Sol. Cells 254 (Jun. 2023) 112238, https://doi.org/10.1016/j. solmat.2023.112238.

- [26] R. Bader, S. Haussener, W. Lipiński, Optical design of multisource high-flux solar simulators, J. Sol. Energy Eng. 137 (2) (Apr. 2015) 021012, https://doi.org/ 10.1115/1.4028702.
- [27] G. Levêque, R. Bader, W. Lipiński, S. Haussener, Experimental and numerical characterization of a new 45 kw\_el multisource high-flux solar simulator, Opt. Express 24 (22) (Oct. 2016) A1360, https://doi.org/10.1364/OE.24.0A1360.
- [28] L. Li, et al., Experimental evaluation of an indirectly-irradiated packed-bed solar thermochemical reactor for calcination–carbonation chemical looping, Chem. Eng. J. 468 (Jul. 2023) 143543, https://doi.org/10.1016/j.cej.2023.143543.
- [29] J. Pottas, L. Li, M. Habib, C.-H. Wang, J. Coventry, W. Lipiński, Optical alignment and radiative flux characterization of a multi-source high-flux solar simulator, Sol. Energy 236 (Apr. 2022) 434–444, https://doi.org/10.1016/j.solener.2022.02.026.
- [30] "Specifications of the High-Flux Solar Furnace," NREL Transforming ENERGY. [Online]. Available: https://www.nrel.gov/csp/facility-hfsf-specs.html.
- [31] A. Ambrosini, A. Boubault, C. K. Ho, L. Banh, and J. R. Lewis, "Influence of application parameters on stability of Pyromark® 2500 receiver coatings," AIP Conf. Proc., vol. 2126, no. July, 2019.
- [32] C.-A. Asselineau, J. Pye, J. Coventry, Exploring efficiency limits for molten-salt and sodium external cylindrical receivers for third-generation concentrating solar power, Sol. Energy 240 (Jul. 2022) 354–375, https://doi.org/10.1016/j. solener.2022.05.001.